Obrabotka metallov (tekhnologiya, oborudovanie, instrumenty) = Metal Working and Material Science. 2025 vol. 27 no. 2 pp. 6–28
ISSN: 1994-6309 (print) / 2541-819X (online)
DOI: 10.17212/1994-6309-2025-27.2-6-28

NSTU NETI

Obrabotka metallov -
Metal Working and Material Science

Journal homepage: http://journals.nstu.ru/obrabotka_metallov

Comparison of ultrasonic surface treatment methods applied to additively manufactured Ti-6Al-4V alloy

Sergey Sundukov [a, *], ***Ravil Nigmetzyanov*** [b], ***Vyacheslav Prikhodko*** [c], ***Dmitry Fatyukhin*** [d], ***Vladimir Koldyushov*** [e]

Moscow Automobile and Road Construction State Technical University (MADI), 64 Leningradsky prospect, Moscow, 125319, Russian Federation

[a] https://orcid.org/0000-0003-4393-4471, sergey-lefmo@yandex.ru; [b] https://orcid.org/0009-0008-1443-7584, lefmo@yandex.ru;
[c] https://orcid.org/0000-0001-8261-0424, prikhodko@madi.ru; [d] https://orcid.org/0000-0002-5914-3415, mitriy2@yandex.ru;
[e] https://orcid.org/0009-0005-6711-6256, v.koldyushov@list.ru

ARTICLE INFO

Article history:
Received: 30 January 2025
Revised: 17 February 2025
Accepted: 17 March 2025
Available online: 15 June 2025

Keywords:
Ultrasonic treatment
Cavitation
Abrasive
Surface deformation
Selective laser melting
Surface roughness
Spherical defects

Funding
This research was funded by the Russian Science Foundation, grant number No. 21-79-00185, https://rscf.ru/project/24-19-00463/

ABSTRACT

Introduction. Selective Laser Melting (*SLM*) of metal powders enables the fabrication of parts with arbitrary geometries, which is unattainable through conventional manufacturing technologies. The main disadvantages of the method include high surface roughness, resulting from metal spattering, spheroidization, partial melting and powder adhesion, as well as difficulties with finishing complex surface areas. One effective approach for processing such parts is the application of ultrasonic liquid technologies, where cavitation bubbles act as working bodies, penetrating and performing work on any area of the surface. **The purpose** of this study is to determine the influence of different types of ultrasonic treatment on the surface properties obtained by selective laser melting through comparative testing. **Materials and methods.** Samples made from *Ti-6Al-4V* titanium alloy, manufactured using selective laser melting on an *EOS M280* machine, were investigated. For ultrasonic treatment, a rod-shaped magnetostrictive vibratory system was used, with the end of the emitter positioned 20 mm from the side surface of the sample. A etching solution (3% HF + 5% HNO_3 + H_2O) was used as a liquid medium to remove the oxide film that hinders the effect of cavitation. Cavitation-erosion (*CET*) treatment, cavitation-abrasive (*CAT*) treatment, and additionally, ultrasonic surface plastic deformation (*USPD*) were performed. After treatment, the surface condition, roughness, and sub-microgeometry were assessed for all samples. The microstructure of the *USPD*-treated samples was also investigated. **Results and discussion.** A high-speed imaging method was used to compare the main mechanisms of interaction with the surface during *CET* and *CAT*. During *CET*, collapsing and pulsating cavitation clusters are observed, located at the points of highest peaks and valleys on the surface. During *CAT*, the micro-cutting action of abrasive particles is added. These particles receive shock waves generated by collapsing bubbles, hit the surface, and undergo oscillatory, rotational, and longitudinal movements. Comparison of the surface condition dynamics revealed that *CET* enables complete removal of surface defects down to the melt tracks. *CAT* removes some surface defects while deforming the remaining ones. During *USPD*, spherical defects are crushed, forming large flat areas. All types of ultrasonic treatment reduce surface roughness: R_a is reduced by 33% during *CET*, by 43% during *CAT*, and by 52% during *USPD*. However, R_{max} is lowest with *CAT*. The microstructure after *USPD* is characterized by a hardened layer with a depth of approximately 100 µm and an increase in microhardness up to 35%. However, after *USPD*, defects in the form of cracks, partially deformed spheres, and the presence of untreated deep surface depressions are formed in the surface layer, which significantly reduces performance characteristics. Therefore, it is advisable to perform *CET* or *CAT* before *USPD* to remove surface defects.

For citation: Sundukov S.K., Nigmetzyanov R.I., Prikhodko V.M., Fatyukhin D.S., Koldyushov V.K. Comparison of ultrasonic surface treatment methods applied to additively manufactured Ti-6Al-4V alloy. *Obrabotka metallov (tekhnologiya, oborudovanie, instrumenty) = Metal Working and Material Science*, 2025, vol. 27, no. 2, pp. 6–28. DOI: 10.17212/1994-6309-2025-27.2-6-28. (In Russian).

Introduction

Layer-by-layer synthesis enables the fabrication of parts with nearly any shape, which reduces the metal consumption and weight of structures and replaces critical assembly processes by manufacturing them entirely in a single operation [1–3].

*** Corresponding author**
Sundukov Sergey K.., Ph.D. (Engineering), Associate Professor
Moscow Automobile and Road Construction
State Technical University (MADI),
64 Leningradsky prospect,
125319, Moscow, Russian Federation
Tel.: +7 926 369-19-70, **e-mail:** sergey-lefmo@yandex.ru

These advantages make additive technologies one of the fastest-growing industries, as demonstrated by the annual increase in the proportion of additively manufactured parts used relative to those produced using traditional technologies [4, 5].

For mechanical engineering, the technologies that enable the production of metal products from powder are of the greatest interest, including selective laser sintering (*SLS*) and selective laser melting (*SLM*).

Production using these methods has a number of significant disadvantages [6–8]:

– low productivity;

– high requirements for the granulometric composition of metal powders;

– the need to print supporting structures, which then have to be removed;

– the need to remove non-melting powder, which prevents manufacturing hollow parts with a closed circuit;

– formation of pores inside the part;

– differences in the mechanical properties of the part in parallel and perpendicular directions relative to the layers of the part;

– high roughness of the resulting surfaces, which, if non-compliant with the specified requirements, requires additional treatment that may not be available for areas with complex geometry.

Since the quality of the surface layer largely determines the operational properties of the product as a whole, high roughness is the main factor preventing the wider use of additive technologies [9].

Regardless of the chemical composition of the metal being fused during selective laser melting, surface roughness is formed as a result of the following factors [10–15]:

– metal splashing from the melt pool;

– spheroidization of liquid metal under the action of surface tension forces when the laser beam is removed from the melting zone;

– incompletely melted powder particles with different adhesion to the surface;

– non-molten powder particles stuck to the surface;

– boundaries between individual layers caused by varying degrees of melting of powder particles located along the boundaries of each layer.

Another significant problem with additive manufacturing is the high probability of pores appearing inside the product, which significantly reduces the strength properties of the product, especially if the pores are close to the surface.

The treatment issues of such products are relevant and are reflected in many scientific papers that propose methods such as laser surface infusion [16], isostatic pressing, which is primarily used to densify the material [17, 18], various types of chemical action [19, 20], coating [21] and surface plastic deformation (*SPD*) [22].

The disadvantage of these methods is that they do not provide for the treatment of complex surfaces. For this purpose, one of the most effective methods is ultrasonic liquid treatment [23–24]. In this case, the working bodies are cavitation bubbles that can penetrate into any surface areas and modify them [25-26].

In modern research on this topic, two types of ultrasonic liquid treatment are considered [27-37]: cavitation-erosion (*CET*) and cavitation-abrasive (*CAT*).

The results in all studies showed a decrease in various roughness parameters and a change in the morphology of the treated surface, manifested as a decrease in the number of defects on the surface. At the same time, the results vary greatly and are achieved with different treatment parameters: time from several minutes [27, 28, 31] to several hours [30, 37], and the amplitudes of ultrasonic vibrations from 5 μm [29] to 80 μm [33–34]. The best results are achieved with *CAT* at a distance of 1–2 mm between the end of the radiator and the treated surface, which is, in fact, dimensional processing and cannot be used for treatment of complex parts, or with *CAT* and *CET* combined with electrochemical polishing at high oscillation amplitudes of 60–80 μm [33–34], which leads to significant heating of the electrolyte, which, in turn, accelerates chemical reactions and makes it difficult to assess the contribution of ultrasound to the resulting effect.

A number of works are devoted to ultrasonic *SPD* [38–47], which leads to a significant reduction in surface roughness, surface hardening and promotes the closure of pores in the subsurface layer. The disadvantage of this method is the difficulties and limitations in the treatment of complex surfaces associated with the inability to bring the indenter of the ultrasonic oscillatory system to hard-to-reach places.

Thus, additional research is required to study in more detail the effect of various types of ultrasonic treatment on the properties of surfaces obtained by additive technologies and to optimize the conditions for the treatment of complex products.

Based on the above, ***the purpose of this work*** is to determine the effect of various types of ultrasonic treatment on the properties of the surface obtained by selective laser melting through comparative tests.

To achieve this purpose, the following ***research objectives*** are set:

– analysis of the main mechanisms of action in ultrasonic treatment methods (*CET*, *CAT*, *SPD*);
– studying the dynamics of surface changes using these methods;
– studying the micro- and submicrogeometry of the treated surface;
– studying the microstructure of the transverse microsection after ultrasonic *SPD*.

Research method

Material and sample production

The samples for experimental studies were cubes of 10×10×10 mm, made by selective laser melting of *Ti-6Al-4V* titanium alloy powder with the chemical composition shown in Table 1.

Table 1

Chemical composition of *Ti-6Al 4V* powder

Element	*Ti*	*Al*	*V*	*Fe*	*Zr*	Bal.
Content, %	89.72	5.3	3.7	0.17	0.04	≈ 1

This material was chosen for research because it is widely used in aerospace engineering, where the production of complex-shaped parts is particularly promising. Furthermore, after selective laser melting, it exhibits pronounced surface defects, as described previously.

The samples were produced at the STANKIN Institute, Department of High-Efficiency Treatment Technologies, using an *EOS M280* machine. The powder had a diameter of 40 µm, and the *SLM* process used a laser beam power of 200 W and a scanning speed of 1,100 mm/s. A total of 25 samples were produced: 5 control samples (without treatment) and 5 samples for each type of treatment under consideration. The treatment schemes are shown in Fig. 2 and Fig. 4.

The lateral surface was selected as the surface for study, as it forms complex elements. Fig. 1, *a* shows a photograph of the surface condition after production, Fig. 1, *b* shows a transverse microsection illustrating defects.

The surface relief is characterized by a sequence of spheres of various diameters. Some of these spheres are the result of spheroidization, while others are partially molten powder or particles of non-molten powder adhering to the surface during the crystallization of the outermost melt tracks.

From the perspective of reducing roughness through further treatment, the spheroidization defects are the most challenging. These spheres are formed from molten tracks of liquid metal and, after crystallization, become almost an integral part of the surface.

Ultrasonic treatment schemes and equipment

Ultrasonic cavitation-erosion treatment (*CET*), cavitation-abrasive treatment (*CAT*), and surface plastic deformation (*SPD*) were used to modify the surface condition.

Preliminary experiments on liquid-based *CET* and *CAT* of *Ti-6Al-4V* samples showed that the alloy's strong surface oxide film results in high cavitation resistance. Consequently, even with prolonged ultrasonic

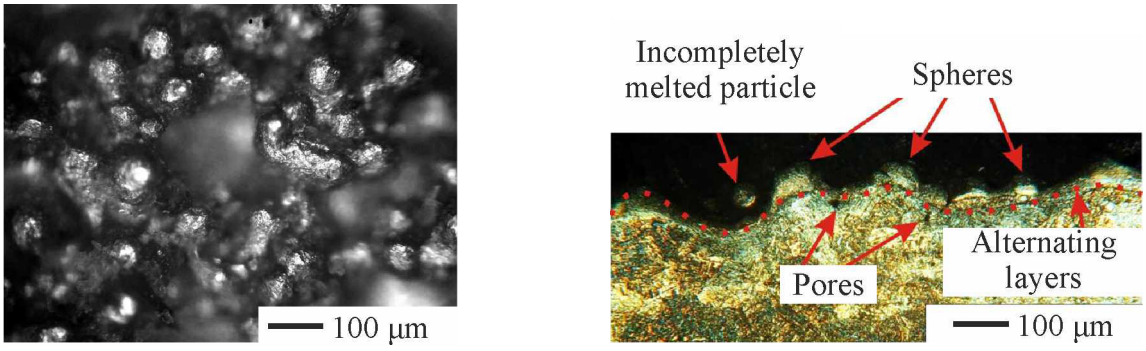

a *b*

Fig. 1. Images showing the condition of the samples side surface:
a – top view; *b* – cross-sectional micrographic image

treatment (1 hour), only a small number of loosely adhered powder particles were removed from the surface, with a negligible effect on the overall surface condition. Therefore, the surface was pre-treated in an etching solution consisting of hydrofluoric and nitric acids, as well as distilled water (3% HF + 5% HNO_3 + H_2O), according to the schemes shown in Fig. 2. To assess the effectiveness of ultrasound exposure, chemical treatment (*CT*) was performed in an etching solution without ultrasonic vibrations (Fig. 2, *a*).

CT was performed by immersing the sample in the etching solution for 30 minutes. Every 10 minutes, the sample was removed, rinsed under running water for 1 minute, dried, and wiped with ethyl alcohol. The side surface was then photographed using a microscope.

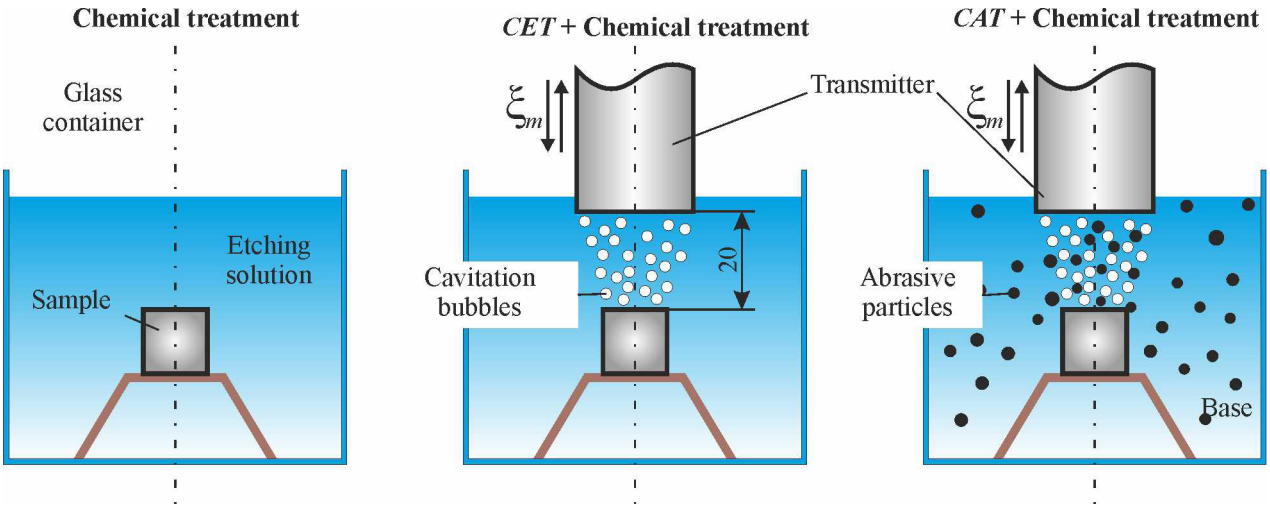

Fig. 2. Schematic diagrams of treatment

The combined processes of *CET* + *CT* and *CAT* + *CT* were carried out by introducing an emitter of the ultrasonic rod oscillatory system *PMS 2.0/22*, consisting of a magnetostrictive transducer, which is a package of *O*-shaped plates made of permendur, and a titanium alloy waveguide soldered to it. The radiator made from *VT-3* has a radiating surface diameter of 30 mm. The distance between the end of the radiator and the treated surface of the sample was 20 mm.

The oscillatory system was powered by a *UZG 2.0/22* ultrasonic generator. The resonant oscillation frequency was f = 19,750 Hz, the oscillation amplitude ξ_m = 20 μm. Under these treatment conditions, the power consumption of the generator was approximately 600 W.

The oscillation amplitude of 20 μm corresponds to high-amplitude treatment conditions, where, in addition to cavitation bubbles, large-scale acoustic currents directed from the end of the radiator to the sample surface make a significant contribution to the treatment. Under the selected experimental conditions, the flow force of the formed streams exceeds the abrasive particles' gravitational force, ensuring

their continuous circulation within that volume and return to the cavitation treatment zone.

Boron carbide powder B_4C was used as an abrasive (Fig. 3), chosen for its high hardness and resistance to chemical attack.

The abrasive powder was added to a level above the treated surface, with a volume concentration of 20%. After the ultrasound was activated, the abrasive was distributed throughout the volume by the acoustic streaming.

To minimize the thermal effects during ultrasonic treatment, a glass container holding an etching solution was placed in a large container with water at room temperature of 20 °C.

The treatment was interrupted at intervals of 1 to 3 minutes to photograph surface changes.

Fig. 3. Boron carbide particles

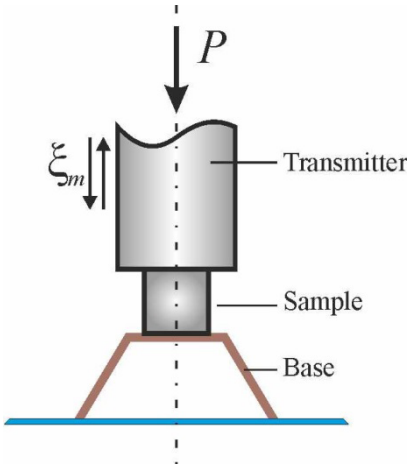

Fig. 4. Scheme of ultrasonic surface plastic deformation

Ultrasonic *SPD* was performed by pressing the end of the oscillatory system against the sample under its own weight ***P*** =70 N (Fig. 4).

The treatment was carried out for 10 seconds while photographing the surface every 2 seconds.

Comparison of surface treatment mechanisms in CET and CAT

To compare the impact mechanisms on the surface during *CET* and *CAT*, high-speed photography of the metal plate treatment in water was performed. The metal plate was also positioned at a distance of 20 mm from the end of the radiator.

The photography was performed using a *Fastec Hispec* camera, capable of recording video clips at frame rate ranging from 500 to 112,000 fps.

To analyze the movement patterns of cavitation bubbles and abrasive particles over the treated surface, video clips were recorded at 5,339 fps, with a field of view of 3.40×3.3 mm.

Subsequently, frame-by-frame processing of the recorded video clips was performed using specialized software provided by the high-speed camera manufacturer.

The results are presented as a sequence of frames starting from the moment the ultrasound was activated. The time indicated in the upper right corner of each frame was calculated as the ratio of the frame number ***N*** (starting from the moment the ultrasound was activated) to the frame rate (***t*** = ***N***/5,339).

Surface structure and roughness studies

During all the above-mentioned types of treatment, the lateral surface of the samples was photographed using a *METAM-RV-22* metallographic microscope.

After ultrasonic *SPD*, a transverse microsection made from the sample was additionally examined to analyze changes in the microstructure resulting from the surface deformation.

After reaching the treatment time beyond which no significant surface changes were observed, the roughness parameters were measured using a *Model 130* profilometer to obtain surface profiles in the form of profilograms. The results were based on the average values from five measurements of the height roughness parameters ***Ra***, ***Rz***, ***Rmax***.

Changes in the sub-microgeometry of surfaces after treatment were evaluated by atomic force microscopy (*AFM*) using a *SMM-2000* scanning multimicroscope with an *MSCT* cantilever having a beam stiffness of 0.1 N/m.

Microhardness was measured using the *Vickers* hardness test method on a *PMT-3* device by indenting the surface with a diamond pyramid under a load of 50 g for 10 seconds. The results were based on the average values from five measurements taken in different locations of the sample.

Results and discussion

Comparison of CET and CAT surface mechanisms

Fig. 5 shows a film diagram of the *CET* process.

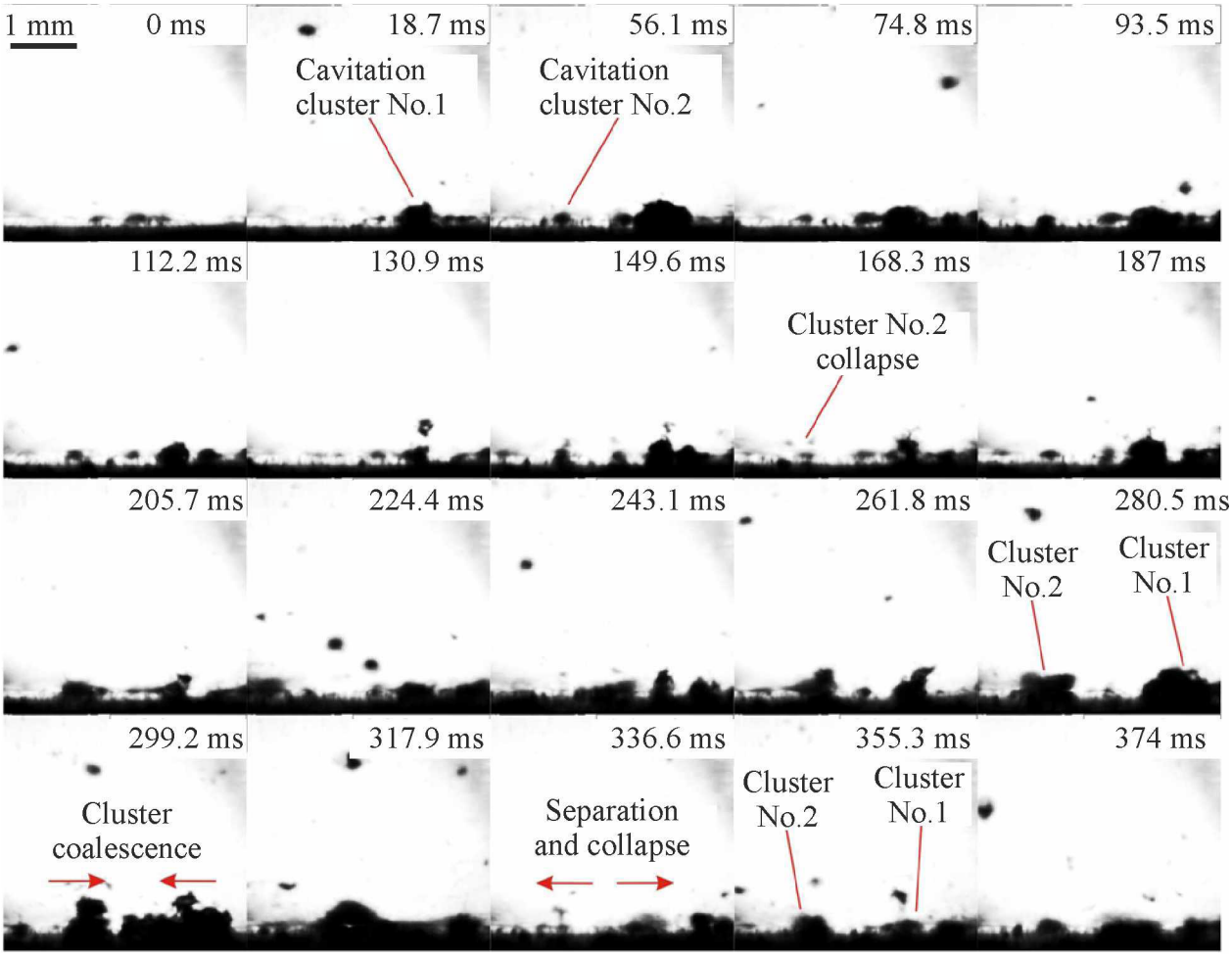

Fig. 5. CET process cinematography (frame rate: 5,339 fps)

At the moment ultrasound is activated, the liquid is subjected to varying compressive and tensile forces corresponding to the oscillation phases of the radiator end. As a result of breaks in liquid continuity, cavitation bubbles are formed. These bubbles oscillate, collapse, combine, and move within the treated volume under the influence of acoustic streams. The most favorable locations for bubble formation and accumulation are various surface irregularities, such as protrusions and depressions of the microrelief.

The first frame shows the formation of cavitation bubbles on the treated surface. This process begins even before the bubbles formed under the radiator are transferred to the surface by the acoustic stream. Over time, the number of bubbles increases, and they combine near the largest surface irregularity, forming a cavitation cluster. Similarly, other clusters form on the surface at different times. The frames illustrate the formation and a portion of the life cycle of two cavitation clusters, which pulsate, absorb cavitation bubbles carried by the acoustic stream, collapse and reform.

The frame corresponding to 168 ms of the treatment process shows the collapse of cluster 2. In the next frame (187 ms), it begins to reform in the same location and reaches its maximum size by 261.8 ms. At 280.5 ms, the two clusters begin to merge. The combined cluster then partially collapses, and the remaining part of the bubbles splits into two (317.9 ms), which return to their previous locations and begin to grow again (336.6–355.3 ms).

As a result, the main mechanism of *CET* is the collapse and pulsation of cavitation bubbles in locations of maximum surface irregularity. From the perspective of treating additive products, this mechanism, on the one hand, helps to remove surface defects; on the other hand, it leads to an increased depth of microrelief depressions.

In *CAT* (Fig. 6), cavitation clusters also form on the surface covered with an abrasive layer at the time when ultrasound is activated. The pulsation of these clusters leads to the separation of abrasive particles (0-18.7 ms). As the clusters grow, the process intensifies, and most abrasive particles are separated from the surface (56.1–112.2 ms). By this time, the acoustic stream and the cavitation bubbles carried by it from the radiator reach the treatment area (130.9 ms), drag the abrasive particles with them, and transfer them back to the surface. This results in a shock effect, which is determined by the speed of movement of the abrasive. This speed can be equal to the stream velocity or significantly increase when a bubble collapses next to an abrasive particle, imparting a pulse via the resulting shock wave (frames after 149.6 ms).

After impacting the surface, a significant number of particles enter the field of action of the clusters, where they oscillate with them, rotate (187 ms), impact the surface during the cluster collapse, and move along the surface (243.1–261.8 ms). In all cases, the surface is subjected to a micro-cutting effect from abrasive particles, which changes the microrelief.

When the power of the acoustic stream escaping to the sides exceeds the forces acting on the abrasive particle, the particle is carried away. Subsequently, the acoustic stream returns under the end of the radiator, from where it is transferred to the surface, where it performs micro-cutting.

At frames 336.6–355.3 ms, the combined effect of cavitation clusters and abrasive particles is more pronounced.

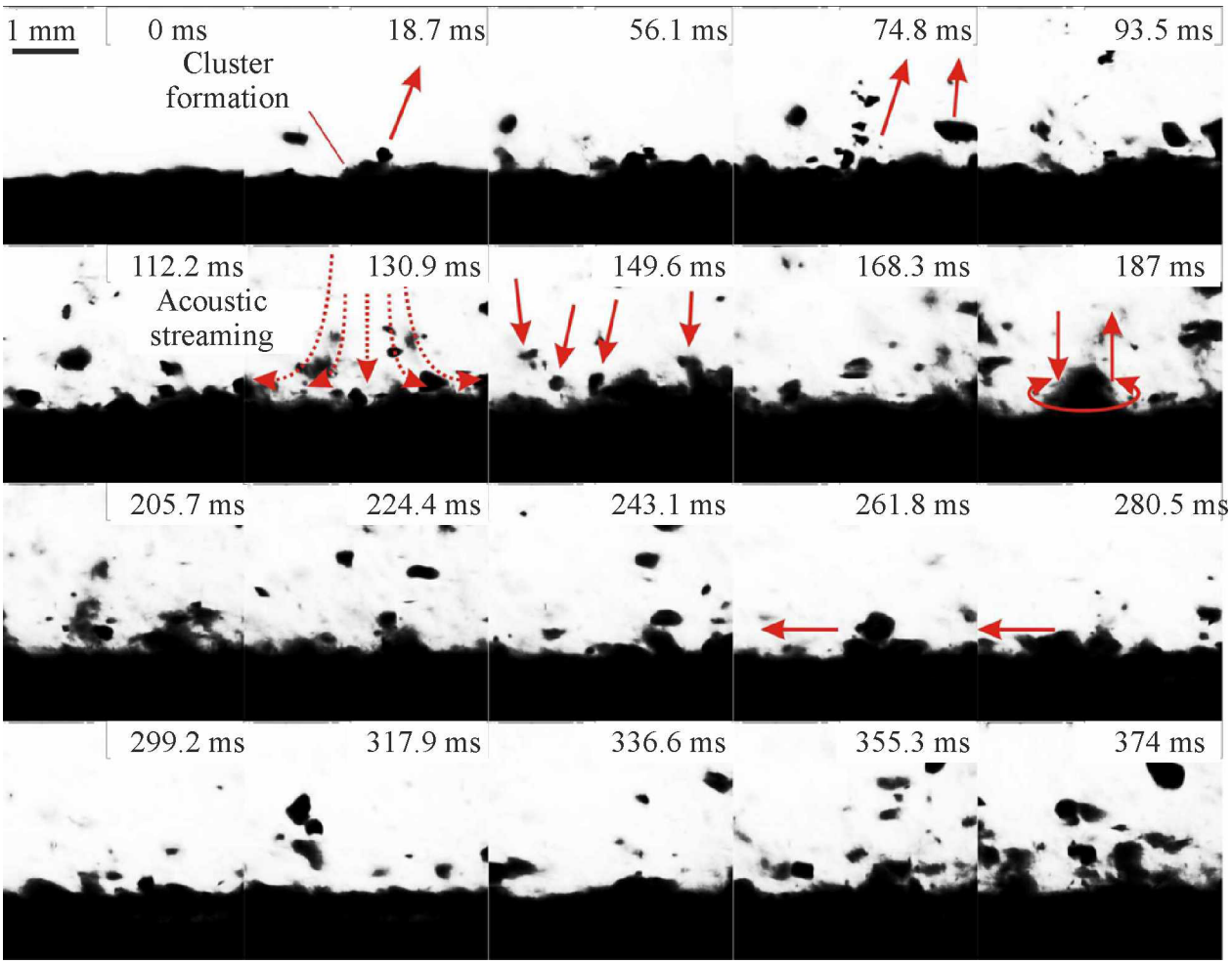

Fig. 6. CAT process cinematography (frame rate: 5,339 fps)

Thus, when an abrasive is added to the liquid, a uniform effect is ensured over all surface areas due to the combined action of cavitation clusters and abrasive particles.

Dynamics of changes in the surface layer during various types of treatment

In *CT*, the oxide film is initially removed by the etching solution. Subsequently, the etching solution begins to interact with the alloy, dissolving the contacting surface areas at a low rate (Fig. 7).

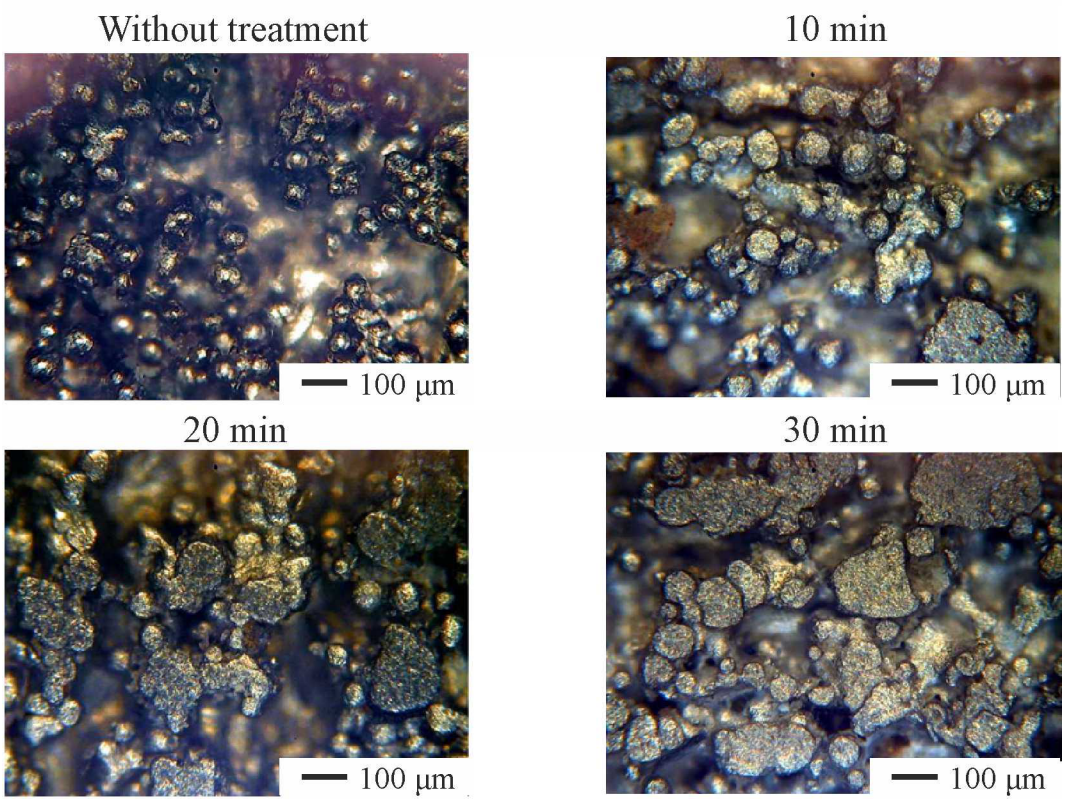

Fig. 7. Dynamics of surface changes during chemical treatment process

During *CT*, the size of the spheres decreases, and the boundaries between spheres in clusters become less distinct, leading to the formation of larger areas. As the *CT* time increases, these areas partially combine to form large areas. Simultaneously, depressions of the surface irregularities are etched, appearing as unfocused regions in the photographs.

When ultrasonic vibrations are introduced into the solution, the dynamics of the treatment change significantly (Fig. 8). Cavitation clusters form and perform work at the locations of the greatest surface irregularity.

When bubbles collapse in these clusters, shock waves and cumulative jets occur, accompanied by instantaneous pressures reaching up to 700 MPa and temperatures up to 4,000 °C [48–49]. As a result of the cumulative effect, plastic deformation of the treated surface occurs [50–51]. In the case of *CET*+*CT*, these instantaneous high temperatures further intensify the chemical reaction at the bubble collapse sites.

Consequently, after 3 minutes of treatment with *CET*+*CT*, the resulting surface is similar to the surface treated with *CT* for 20 minutes, indicating an acceleration of the process by almost a factor of 7.

The main difference between *CET*+*CT* and *CT* alone is that, with increasing treatment time, the number of protrusions of irregularities decreases, and the unfocused area increases in each subsequent photo, indicating the removal of surface defects. Starting from minute 7 of treatment, a portion of the surface becomes clearly visible, showing an alternation of powder melting tracks. After 15 minutes of treatment, defects such as metal splashes and spheres are completely removed from the surface.

Adding abrasive particles during *CAT* also changes the nature of the treatment (Fig. 9).

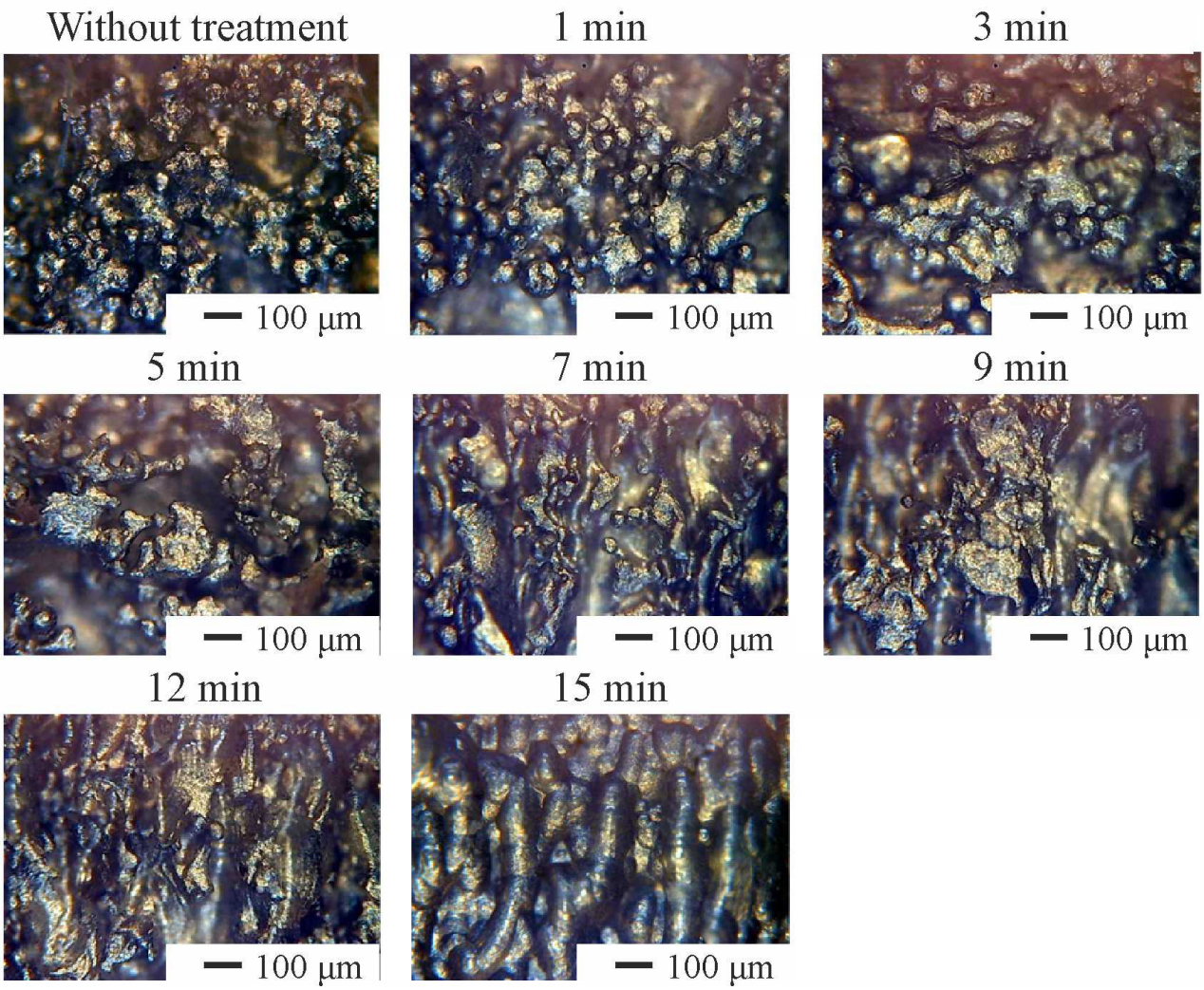

Fig. 8. Dynamics of surface changes during CET + Chemical treatment

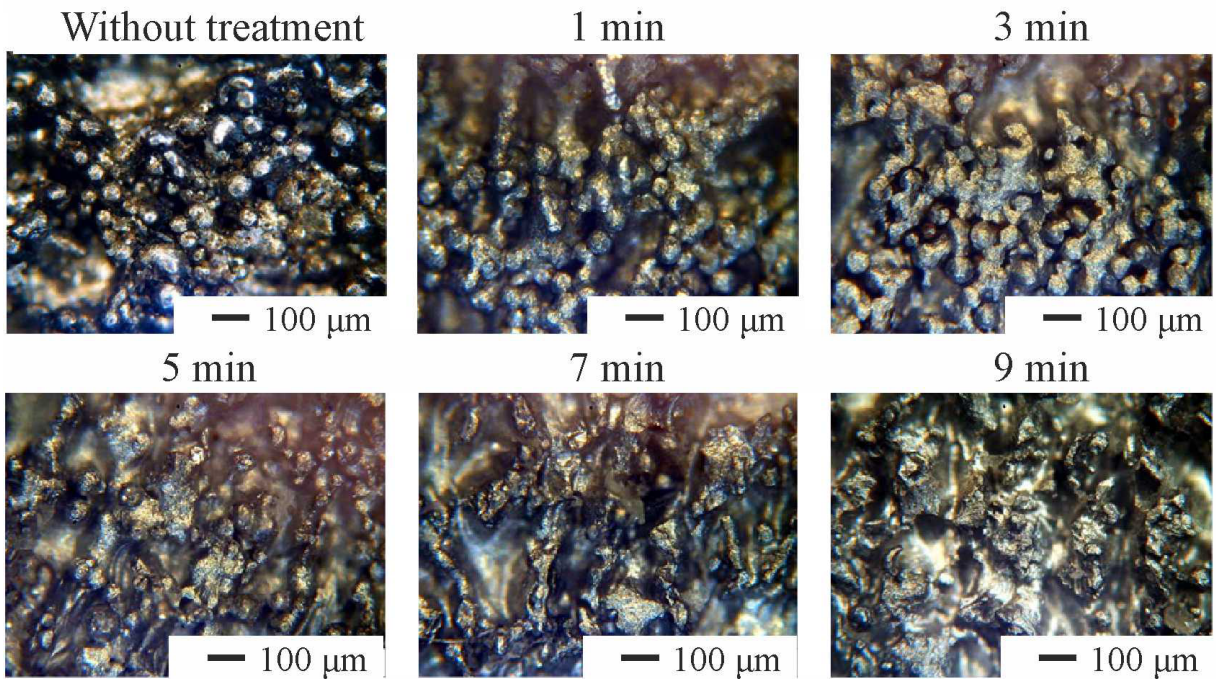

Fig. 9. Dynamics of surface changes during *CAT* + Chemical treatment

In this case, a significant portion of the energy generated by bubble collapse is transferred to the abrasive particles, which, upon impacting the surface, perform micro-cutting. This redistribution of energy changes the nature of the treatment towards a predominantly mechanical abrasive process.

After one minute of *CAT*, a significant portion of the spheres is removed. The formation of sites characteristic of both *CT* and *CET+CT* is almost imperceptible. This suggests that defects with poor adhesion are preferentially removed first due to the impact of the abrasive. Further, the effect of *CET+CT* is that *CT* etches defects, reducing the strength of their adhesion to the surface, after which they are removed by the abrasive. Defects with high adhesion strength, primarily those resulting from spheroidization, deform upon impact of the abrasive, leading to a reduction in the height of the relief irregularities.

As a result, after 10 minutes of treatment with *CAT*, the surface consists of significantly deformed spheres and melting tracks, also exhibiting traces of abrasive action.

The mechanism of ultrasonic *SPD* involves the plastic deformation of surface irregularities (Fig. 10).

Under the action of a force applied normally to the surface, the protrusions of irregularities deform. The height of the spheres decreases with the formation of a flattened area, while they simultaneously grow in width and begin to touch other spheres. Consequently, deformed areas of a sufficiently large size are formed on the surface. With continued treatment, the spheres located below begin to deform, and the area of the deformed regions increases. The largest area is achieved after approximately 10 seconds of treatment. As the treatment time increases further, no significant changes occur, likely due to the achievement of the maximum degree of deformation.

Despite the significant effect of surface smoothing, treatment of microrelief depressions is not achievable with this method, as illustrated in all the photos.

Despite the significant effect of surface smoothing, treatment of microrelief depressions is not available for this method, which is illustrated in all the photos.

The analysis of microstructure changes is presented below.

Analysis of surface roughness changes

The surface changes resulting from the considered treatment methods lead to change in surface roughness. Profilometer traces, each 2.5 mm long, and height roughness parameters for all treatment types are presented in Table 2.

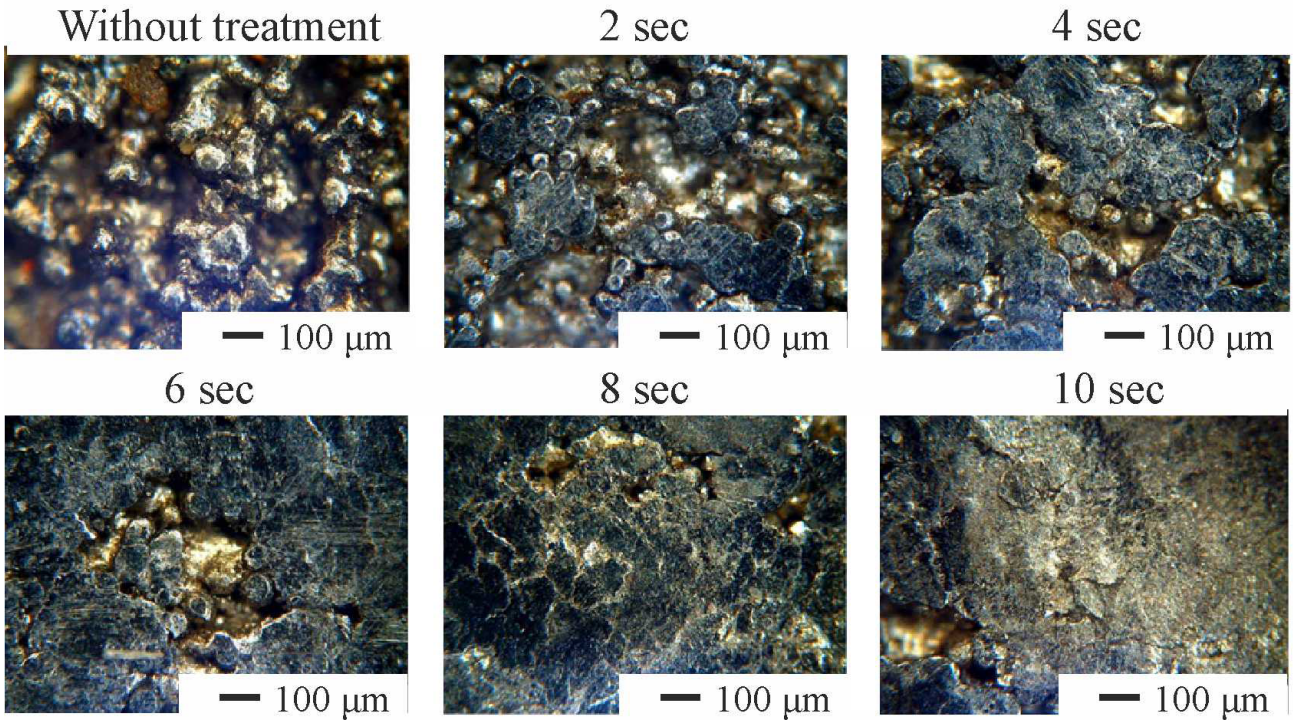

Рис. 10. Dynamics of surface changes during ultrasonic *SPD*

Table 2

Surface microgeometry

Treatment	Surface profile section (2.5 mm)	Roughness parameters
Without Treatment	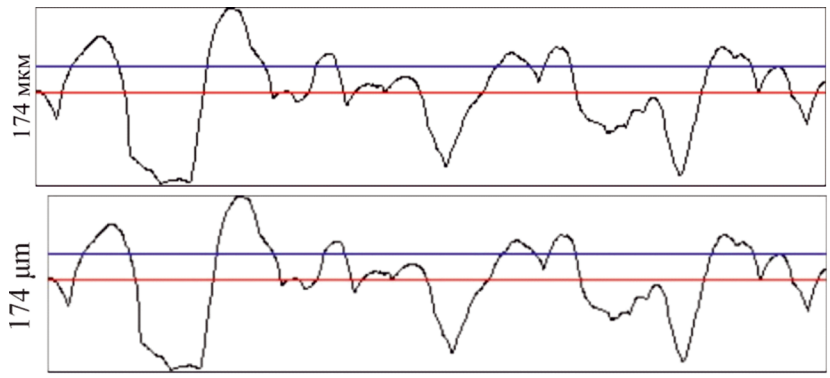	R_a = 28,6 R_z = 114
Chemical treatment (30 min)	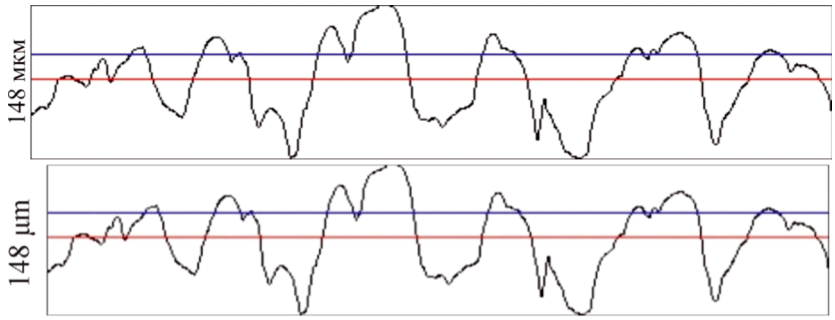	R_a = 23,2 R_z = 103
CET and chemical treatment (15 min)	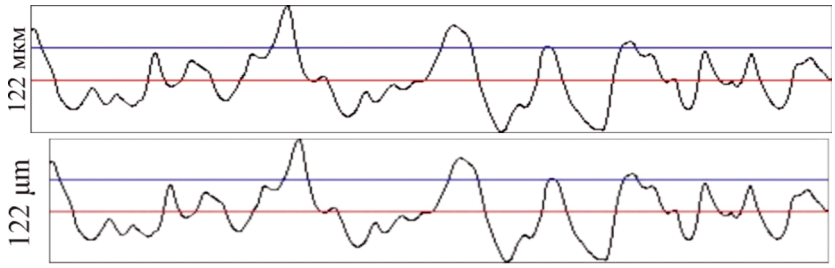	R_a = 19,3 R_z = 94,2
CAT and chemical treatment (10 min)	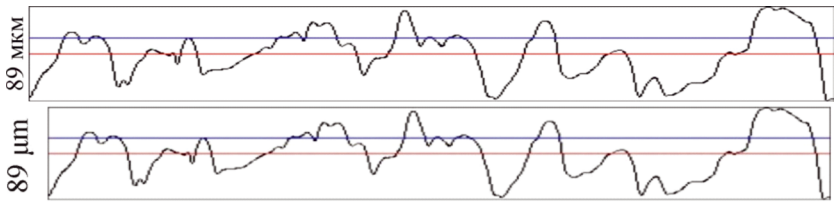	R_a = 16,2 R_z = 80,5
USPD (10 sec)	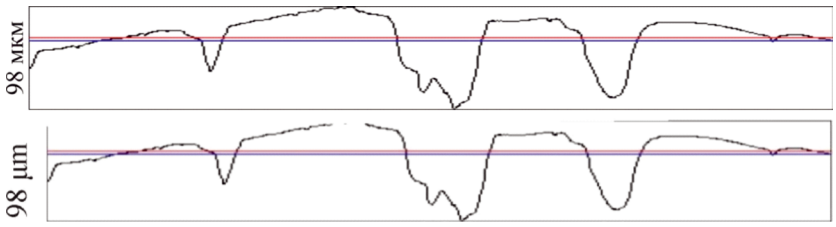	R_a = 13,6 R_z = 76,3

The profile of the micro-irregularities of the control sample consists of alternating protrusions with rounded peaks and depressions, with a predominance of protrusions. The maximum profile height is *Rmax* = 174 µm.

Following *CT*, the profile exhibits a similar relief but with a reduced height of the protrusions and a slightly increased width of the depressions. The arithmetic mean deviation of the profile, *Ra*, decreases from 28.6 to 23.2 µm.

Ultrasonic treatment methods result in significant profile changes, both in the shape of the profilogram and in the numerical values of the roughness parameters.

After *CET+CT*, the surface profile is leveled and consists of similarly sized protrusions and depressions. This is due to the absence of spherical defects on the surface. The *Ra* parameter decreases to 19.3 μm.

The profile after *CAT+CT* is characterized by fewer depressions and a larger number of protrusions deformed by the abrasive. *Ra* = 16.2 μm, representing a decrease of 43.5%. Additionally, the profilogram after this treatment method exhibits the lowest maximum profile height of 89 μm.

The surface relief after ultrasonic *SPD*, due to the presence of large, flat areas, has the lowest value of *Ra* = 13.6 μm. However, the difference in the height of the protrusions and the depth of the depressions reaches 98 μm, which is greater than with *CAT+CT*. This indicates that combined cavitation and abrasive action is a more effective method for reducing surface protrusion height.

Assessment of changes in the submicrostructure

Three-dimensional images of the surface topography, measuring 308×308 nm (Fig. 11), were obtained by atomic force microscopy (*AFM*) using the Constant Height method. This method maintains a constant distance between the cantilever and the surface under study during scanning. These images allow assessment of the formation mechanisms of the studied surfaces.

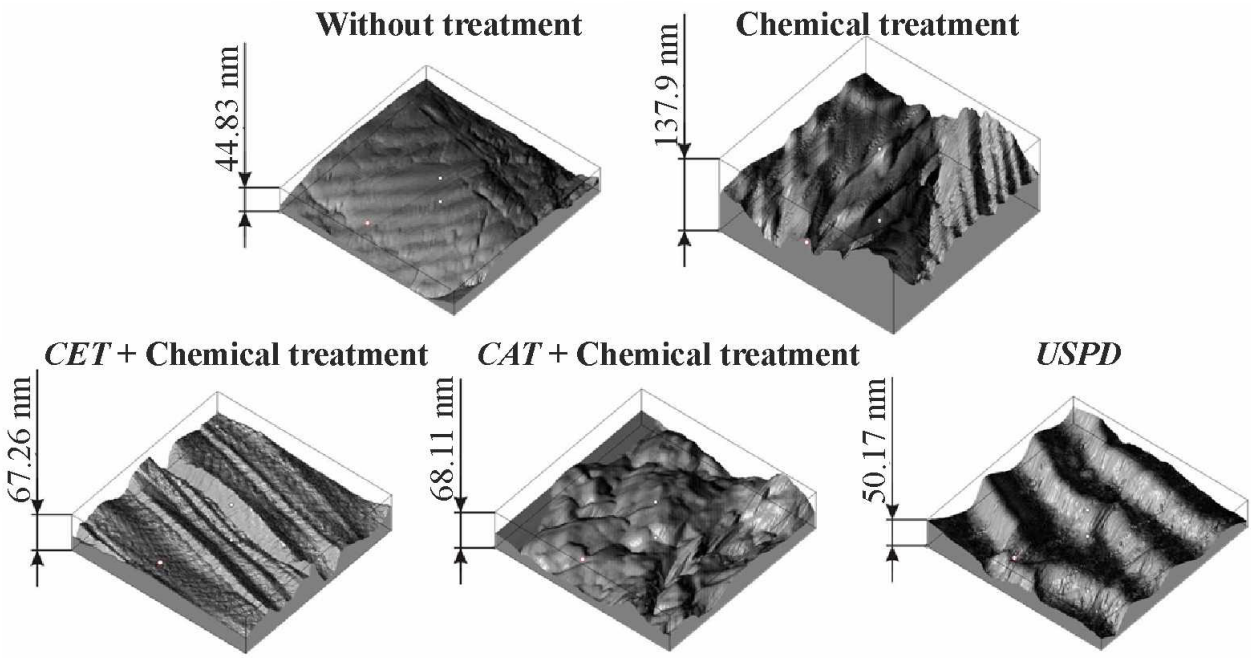

Fig. 11. AFM images of surfaces (308×308 nm)

As a result of the flattening of spherical irregularities, the surface profile is leveled and consists of large, rectilinear sections alternating with depressions. In this case, the surface layer acquires several defects (hereafter, the defect number corresponds to the designation in Fig. 12):

– discontinuity of metal at the points of contact of deformed spheres, appearing as vertical cracks;
– discoloration of spheres under the influence of vibrations and shock loading;
– partially deformed spheres with poor adhesion to the surface;
– untreated deep depressions that increase roughness and may contain adhering powder particles.

The deformed layer after ultrasonic *SPD* is approximately 90 to 100 μm thick. Without treatment, the sample has a lamellar microstructure typical of *Ti-6Al-4V* alloy, which is the same in the surface layer (Fig. 13, *a*) and the base metal (Fig. 13, *b*). After treatment, the microstructure of the material shows clearly marked traces of deformation (Fig. 13, *c*, *d*). Furthermore, the area of the surface without spheres (Fig. 13, *c*) is deformed to a greater extent than the area with spheres (Fig. 13, *g*), where the spheres themselves are deformed much more intensively than the underlying metal layer.

The submicrostructure of the control sample has a slightly rounded shape with undulating steps, which is probably a consequence of the crystallization of a spherical particle.

The *AFM* image after *CT* shows a region with a boundary between a sphere (right corner of the image), which exhibits pronounced steps after etching, and a portion of the surface formed during normal crystallization of the melt track.

After *CET+CT*, the banded submicrostructure results from directional heat dissipation during the crystallization of the melt track.

The surface after *CAT+CT* differs from the others in its chaotic structure, formed by periodic exposure to abrasive particles.

Wide steps, resembling surges, indicate the flow of metal perpendicular to the direction of deformation during ultrasonic *SPD*.

Examination of the hardened layer after ultrasonic SPD

The changes in the surface profile (Fig. 12) correspond to the surface profilometer traces presented in Table 2.

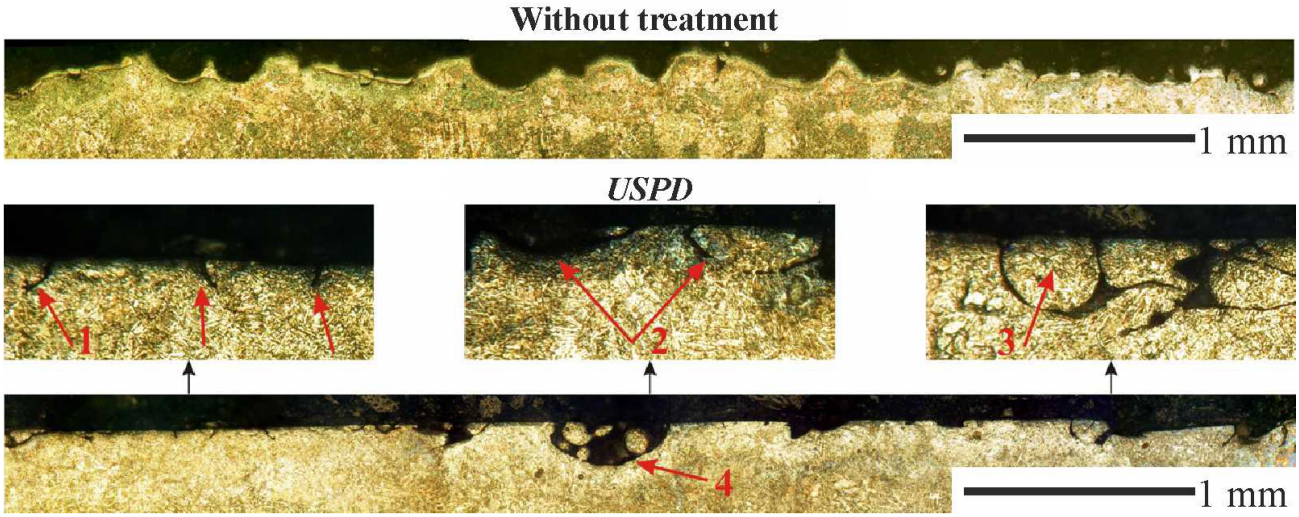

Fig. 12. Surface Profile in Cross-Sectional Micrograph:
1, 2, 3, 4 – surface layer defects

The deformed layer is characterized by high microhardness (Fig. 14). The maximum hardening is achieved closer to the edge of the surface layer, reaching approximately 35 %. As the distance from the surface increases, the microhardness gradually decreases, reaching the base metal level after 100 μm.

As a result, ultrasonic *SPD* leads to a significant reduction in surface roughness and the creation of a hardened layer. However, the resulting surface defects can significantly decrease the performance characteristics of the part. Therefore, it is advisable to perform ultrasonic *SPD* after removing surface defects using the aforementioned methods of *CAT+CT* or *CET+CT*.

Description of the mechanisms of action during ultrasonic treatment

Three-dimensional images of the sample surfaces, obtained by extended depth of field microscopy, are shown in Fig. 15. These images visualize the surface changes that occur during various types of treatment.

Changes in the surface condition are determined by the type of ultrasonic treatment used and the corresponding mechanisms of action, schematically shown in Fig. 16.

In the case of *CET*, the primary effect is exerted by cavitation clusters formed at locations of greatest surface inhomogeneity, which are spherical defects and depressions of micro-irregularities. The pressure and temperature formed during the collapse of clusters lead to plastic deformation of the surface, removal of spheres, and an increased depth of depressions. Since the depressions in the samples under consideration are mainly formed between the spheres, the roughness will decrease during treatment until all the spheres

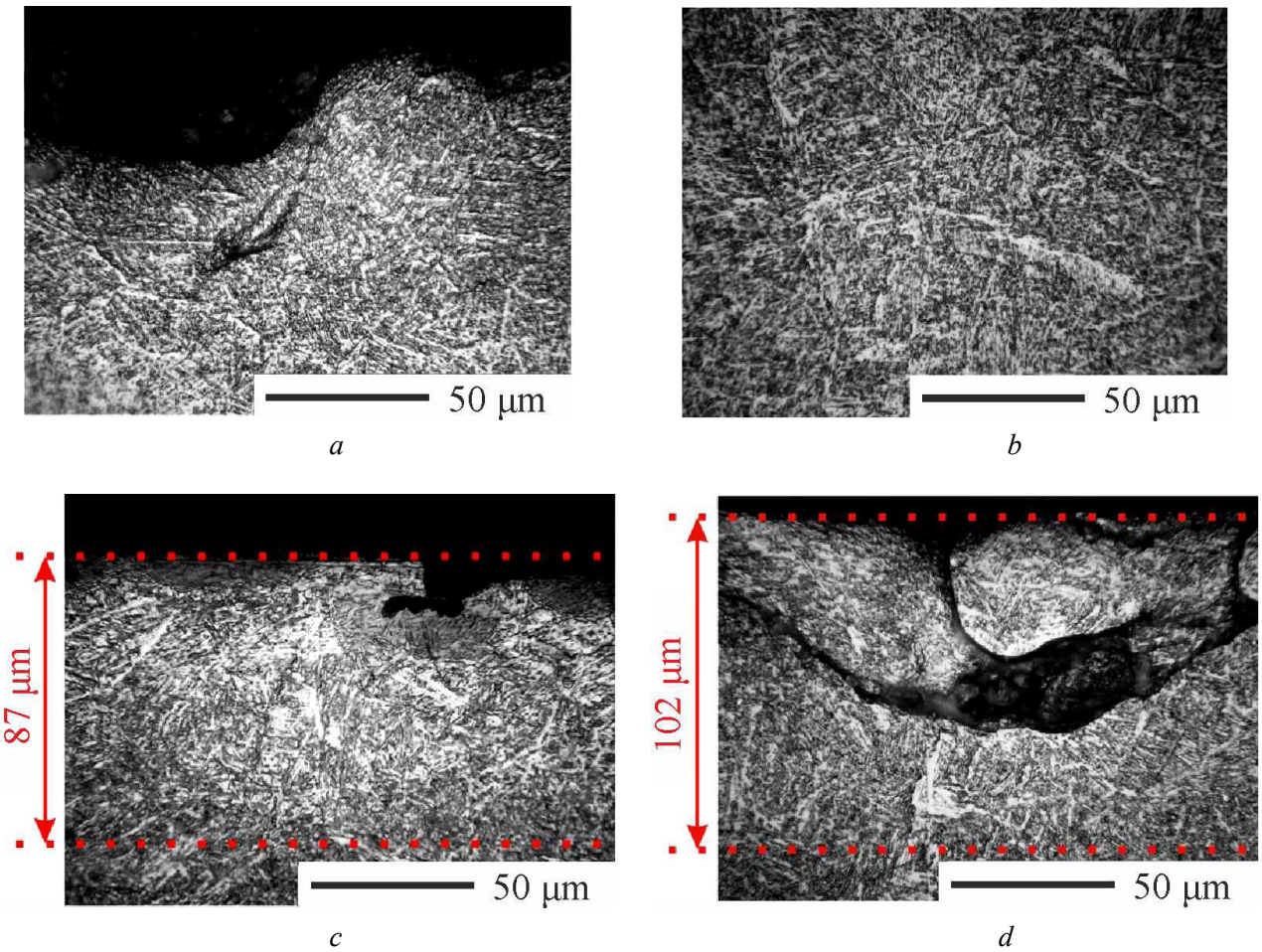

Fig. 13. Microstructures:
a – edge of control sample; *b* – bulk material; *c* – edge of sample after *USPD*; *d* – deformed spheres after *USPD*

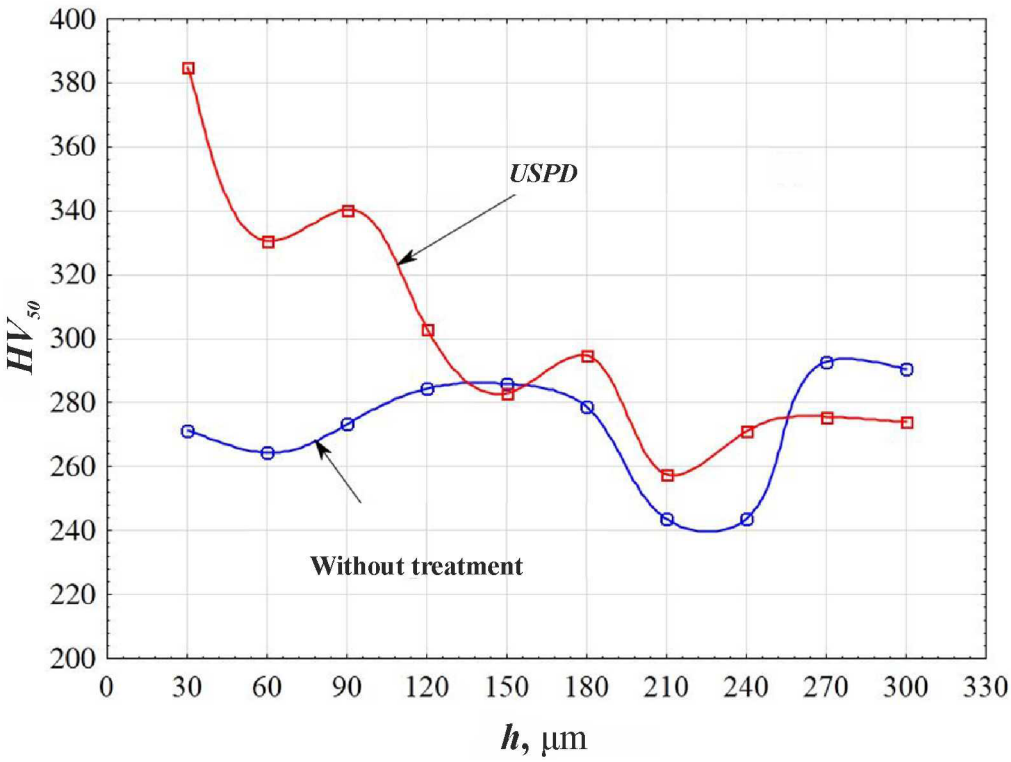

Fig. 14. Microhardness profiles of samples

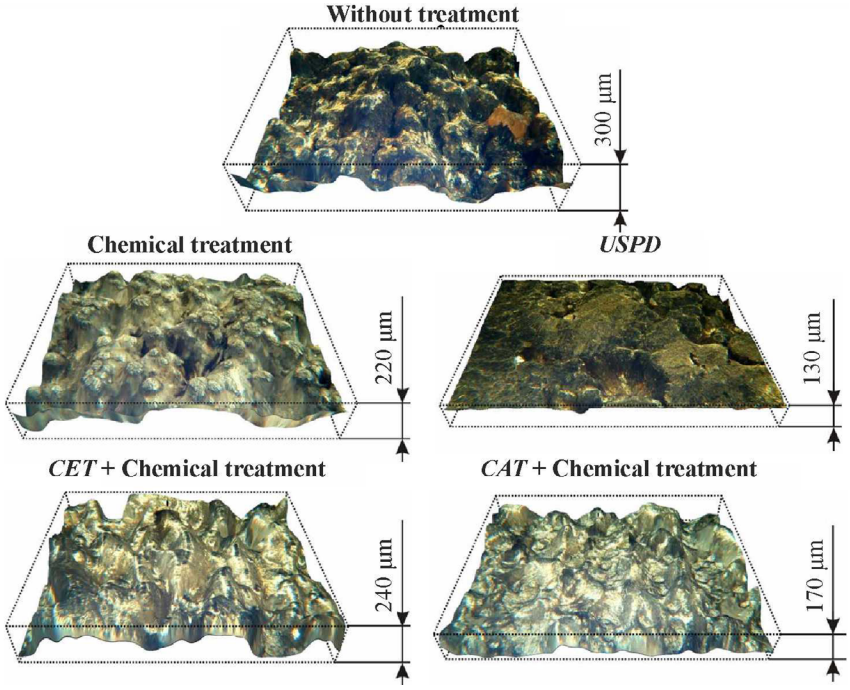

Fig. 15. Three-dimensional images of surfaces after various treatments

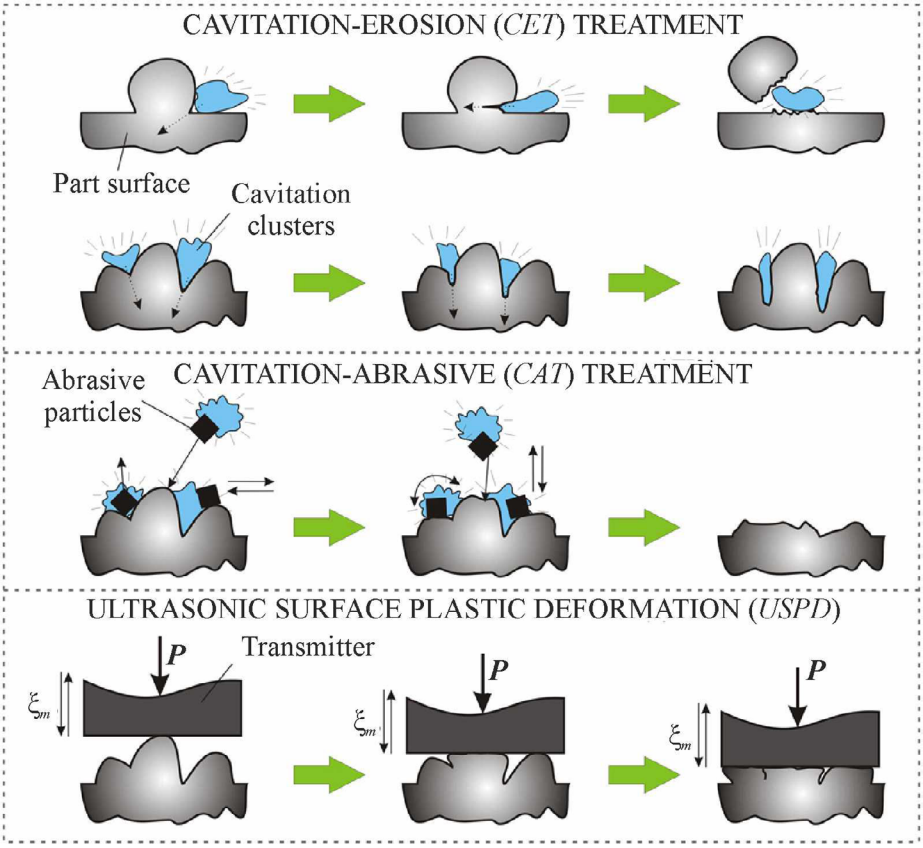

Fig. 16. Schematic illustration of surface change dynamics during various types of ultrasonic treatment

are removed. The combination of *CET*+*CT* significantly speeds up the treatment process by removing the strong oxide film and intensifying chemical etching due to high temperatures.

When clusters collapse during the *CAT* process, the resulting shock waves are transferred to abrasive particles that strike the surface, exerting a micro-cutting effect. In addition, the particles, when interacting

with the cluster, undergo oscillatory, rotational, and longitudinal movements along the surface, deforming its irregularities.

In ultrasonic *SPD*, the main mechanism is the deformation of the protrusions of micro-irregularities and spheres under the action of a high-frequency micro-shock load.

Conclusions

Comparative studies of various types of ultrasonic treatment of *Ti-6Al-4V* titanium alloy samples obtained by selective laser melting have shown the following:

– the microgeometry of the sample surface is a set of spherical defects caused by manufacturing features, resulting in high roughness;

– liquid processing methods, *CET* and *CAT*, are effective in the etchant environment (3% HF + 5% $HNO_3 + H_2O$), which allows for the removal of the oxide film;

– a comparison of *CET* and *CAT* using high-speed imaging showed that with *CET*, cavitation bubbles cluster at locations of greatest surface irregularities where work is carried out. With *CAT*, clusters and abrasive particles act together, which, in addition to impacting the surface, undergo oscillatory, rotational, and longitudinal movements, deforming the protrusions of micro-irregularities;

– high pressures and temperatures that occur during the collapse of cavitation bubbles significantly accelerate chemical etching at the collapse sites;

– *CET*+*CT* for 15 minutes leads to the complete removal of all spherical surface defects, resulting in a surface that is an alternation of melt tracks;

– with *CAT*+*CT*, the resulting pressures and temperatures are largely transferred to abrasive particles, which, when accelerated, perform micro-cutting actions, resulting in the removal and/or deformation of some of the defects;

– ultrasonic *SPD* treatment leads to the flattening of surface defects and the formation of large, flat areas on the surface;

– with all the considered types of ultrasonic treatment, surface roughness decreases: *Ra* decreases by 33% with *CET*+CT, by 43% with *CAT*+*CT*, and by 52% with ultrasonic *SPD*. However, the greatest height of irregularities, *Rmax*, is the least with *CAT*+*CT*;

– analysis of the microstructure after *SPD* reveals a hardened layer with a depth of approximately 100 μm and an increase in microhardness of up to 35%;

– the primary disadvantage of *SPD* is the formation of defects in the surface layer, including cracks, partially deformed spheres, and the presence of untreated deep surface depressions;

– prior to *SPD*, it is advisable to carry out *CET*+*CT* or *CAT*+*CT* to remove existing surface defects.

References

1. Peng X., Kong L., Fuh J.Y.H., Wang H. A review of post-processing technologies in additive manufacturing. *Journal of Manufacturing and Materials Processing*, 2021, vol. 5 (2), p. 38. DOI: 10.3390/jmmp5020038.

2. Sundukov S.K. *Ul'trazvukovye tekhnologii v protsessakh polucheniya neraz"emnykh soedinenii* [Ultrasonic technologies in the processes of obtaining permanent connections]. Moscow, Tekhpoligraftsentr Publ., 2023. 263 p. ISBN 978-5-94385-209-1.

3. Grigor'ev S.N., Tarasova T.V. Vozmozhnosti tekhnologii additivnogo proizvodstva dlya izgotovleniya slozhnoprofil'nykh detalei i polucheniya funktsional'nykh pokrytii iz metallicheskikh poroshkov [Potential of additive manufacturing technology for manufacturing complex-shaped parts and obtaining functional coatings from metal powders]. *Metallovedenie i termicheskaya obrabotka metallov = Metal Science and Heat Treatment*, 2015, no. 10 (724), pp. 5–10.

4. Metel A., Tarasova T., Gutsaliuk E., Khmyrov R., Egorov S., Grigoriev S. Possibilities of additive technologies for the manufacturing of tooling from corrosion-resistant steels in order to protect parts surfaces from thermochemical treatment. *Metals*, 2021, vol. 11 (10), p. 1551. DOI: 10.3390/met11101551.

5. Magnien J., Cosemans P., Nutal N., Kairet T. Current surface issues in additive manufacturing. *Plasma Processes and Polymers*, 2020, vol. 17 (1), p. 1900154. DOI: 10.1002/ppap.201900154.

6. Tarasova T.V., Nazarov A.P., Prokof'ev M.V. Effect of the regimes of selective laser melting on the structure and physicomechanical properties of cobalt-base superalloys. *The Physics of Metals and Metallography*, 2015, vol. 116, pp. 601–605. DOI: 10.1134/S0031918X15060101.

7. Aleksandrov V.A., Fatyukhin D.S., Sundukov S.K., Filatova A.A. Ultrasonic methods for improving object surface quality prepared by corrosion-resistant steel powder selective laser melting. *Metal Science and Heat Treatment*, 2018, vol. 60, pp. 381–386. DOI: 10.1007/s11041-018-0287-1.

8. Konov S.G., Kotoban D.V., Sundukov S.K., Fatyukhin D.S. Perspektivy primeneniya ul'trazvukovykh tekhnologii v additivnom proizvodstve [Prospects for the application of ultrasonic technology in additive manufacturing]. *Naukoemkie tekhnologii v mashinostroenii = Science Intensive Technologies in Mechanical Engineering*, 2015, no. 9 (51), pp. 28–34.

9. Tang C., Tan J.L., Wong C.H. A numerical investigation on the physical mechanisms of single track defects in selective laser melting. *International Journal of Heat and Mass Transfer*, 2018, vol. 126, pt. B, pp. 957–968. DOI: 10.1016/j.ijheatmasstransfer.2018.06.073.

10. Zhang B., Li Y., Bai Q. Defect formation mechanisms in selective laser melting: a review. *Chinese Journal of Mechanical Engineering*, 2017, vol. 30, pp. 515–527. DOI: 10.1007/s10033-017-0121-5.

11. Nasab M.H., Gastaldi D., Lecis N., Vedani M. On morphological surface features of the parts printed by selective laser melting (SLM). *Additive Manufacturing*, 2018, vol. 24, pp. 373–377. DOI: 10.1016/j.addma.2018.10.011.

12. Singla A.K., Banerjee M., Sharma A., Singh J., Bansal A., Gupta M.K., Khanna N., Shahi A.S., Goyal D.K. Selective laser melting of Ti6Al4V alloy: process parameters, defects and post-treatments. *Journal of Manufacturing Processes*, 2021, vol. 64, pp. 161–187. DOI: 10.1016/j.jmapro.2021.01.009.

13. Bai Y., Zhao C., Wang D., Wang H. Evolution mechanism of surface morphology and internal hole defect of 18Ni300 maraging steel fabricated by selective laser melting. *Journal of Materials Processing Technology*, 2022, vol. 299, p. 117328. DOI: 10.1016/j.jmatprotec.2021.117328.

14. Li C., Liu D., Liu G., Liu Sh., Jin X., Bai Y. Surface characteristics enhancement and morphology evolution of selective-laser-melting (SLM) fabricated stainless steel 316L by laser polishing. *Optics & Laser Technology*, 2023, vol. 162, p. 109246. DOI: 10.1016/j.optlastec.2023.109246.

15. Shi X., Yan C., Feng W., Zhang Y., Leng Z. Effect of high layer thickness on surface quality and defect behavior of Ti-6Al-4V fabricated by selective laser melting. *Optics & Laser Technology*, 2020, vol. 132, p. 106471. DOI: 10.1016/j.optlastec.2020.106471.

16. Giorleo L., Ceretti E., Giardini C. Ti surface laser polishing: effect of laser path and assist gas. *Procedia CIRP*, 2015, vol. 33, pp. 446–451. DOI: 10.1016/j.procir.2015.06.102.

17. Kumar A.Y., Bai Y., Eklund A., Williams C.B. The effects of Hot Isostatic Pressing on parts fabricated by binder jetting additive manufacturing. *Additive Manufacturing*, 2018, vol. 24, pp. 115–124. DOI: 10.1016/j.addma.2018.09.021.

18. Popov V., Katz-Demyanetz A., Garkun A., Muller G., Strokin E., Rosenson H. Effect of Hot Isostatic Pressure treatment on the Electron-Beam Melted Ti-6Al-4V specimens. *Procedia Manufacturing*, 2018, vol. 21, pp. 125–132. DOI: 10.1016/j.promfg.2018.02.102.

19. Łyczkowska E., Szymczyk P., Dybała B., Chlebus E. Chemical polishing of scaffolds made of Ti–6Al–7Nb alloy by additive manufacturing. *Archives of Civil and Mechanical Engineering*, 2014, vol. 14 (4), pp. 586–594. DOI: 10.1016/j.acme.2014.03.001.

20. Jain S., Corliss M., Tai B., Hung W.N. Electrochemical polishing of selective laser melted Inconel 718. *Procedia Manufacturing*, 2019, vol. 34, pp. 239–246. DOI: 10.1016/j.promfg.2019.06.145.

21. Slegers S., Linzas M., Drijkoningen J., D'Haen J., Reddy N.K., Deferme W. Surface roughness reduction of additive manufactured products by applying a functional coating using ultrasonic spray coating. *Coatings*, 2017, vol. 7 (12), p. 208. DOI: 10.3390/coatings7120208.

22. Hosseinzadeh A., Radi A., Richter J., Wegener T., Sajadifar S.V., Niendorf T., Yapici G.G. Severe plastic deformation as a processing tool for strengthening of additive manufactured alloys. *Journal of Manufacturing Processes*, 2021, vol. 68, pt. A, pp. 788–795. DOI: 10.1016/j.jmapro.2021.05.070.

23. Nigmetzyanov R.I., Sundukov S.K., Fatyukhin D.S., Grib V.V., Kartsov S.K. Additive manufacturing with ultrasound. *Russian Engineering Research*, 2017, vol. 37, pp. 1070–1073. DOI: 10.3103/S1068798X17120140.

24. Sundukov S.K. Ultrasonic vibration mechanism in making permanent joints. *Steel in Translation*, 2024, vol. 54, pp. 10–15. DOI: 10.3103/S0967091224700190.

25. Grigoriev S.N., Metel A.S., Tarasova T.V., Filatova A.A., Sundukov S.K., Volosova M.A., Okunkova A.A., Melnik Y.A., Podrabinnik P.A. Effect of cavitation erosion wear, vibration tumbling, and heat treatment on additively manufactured surface quality and properties. *Metals*, 2020, vol. 10 (11), p. 1540. DOI: 10.3390/met10111540.

26. Metel A.S., Grigoriev S.N., Tarasova T.V., Filatova A.A., Sundukov S.K., Volosova M.A., Okunkova A.A., Melnik Y.A., Podrabinnik P.A. Influence of postprocessing on wear resistance of aerospace steel parts produced by laser powder bed fusion. *Technologies*, 2020, vol. 8 (4), p. 73. DOI: 10.3390/technologies8040073.

27. Tan K.L., Yeo S.H. Surface modification of additive manufactured components by ultrasonic cavitation abrasive finishing. *Wear*, 2017, vol. 378–379, pp. 90–95. DOI: 10.1016/j.wear.2017.02.030.

28. Tan K.L., Yeo S.H. Surface finishing on IN625 additively manufactured surfaces by combined ultrasonic cavitation and abrasion. *Additive Manufacturing*, 2020, vol. 31, p. 100938. DOI: 10.1016/j.addma.2019.100938.

29. Wang J., Zhu J., Liew P.J. Material removal in ultrasonic abrasive polishing of additive manufactured components. *Applied Sciences*, 2019, vol. 9 (24), p. 5359. DOI: 10.3390/app9245359.

30. Tan W.X., Tan K.W., Tan K.L. Developing high intensity ultrasonic cleaning (HIUC) for post-processing additively manufactured metal components. *Ultrasonics*, 2022, vol. 126, p. 106829. DOI: 10.1016/j.ultras.2022.106829.

31. Goh K.W.S., Tan K.L., Yeo S.H. Hybrid ultrasonic cavitation abrasive peening and electrochemical polishing on additively manufactured AlSi10Mg components. *Proceedings of the 3rd International Conference on Advanced Surface Enhancement (INCASE) 2023*. Singapore, Springer, 2023, pp. 59–66. DOI: 10.1007/978-981-99-8643-9_7.

32. Sun M., Toyserkani E. A novel hybrid ultrasound abrasive-driven electrochemical surface finishing technique for additively manufactured Ti6Al4V parts. *Inventions*, 2024, vol. 9 (2), p. 45. DOI: 10.3390/inventions9020045.

33. Wang B., Castellana J., Melkote S.N. A hybrid post-processing method for improving the surface quality of additively manufactured metal parts. *CIRP Annals*, 2021, vol. 70 (1), pp. 175–178. DOI: 10.1016/j.cirp.2021.03.010.

34. Jeon J.H., Panpalia N., Rashid A., Melkote S.N. Effect of electropolishing on ultrasonic cavitation in hybrid post-processing of additively manufactured metal surfaces. *Journal of Manufacturing Processes*, 2024, vol. 120, pp. 703–711. DOI: 10.1016/j.jmapro.2024.04.092.

35. Wang Q., Vohra M.S., Bai S., Yeo S.H. Rotary ultrasonic-assisted abrasive flow finishing and its fundamental performance in Al6061 machining. *The International Journal of Advanced Manufacturing Technology*, 2021, vol. 113, pp. 473–481. DOI: 10.1007/s00170-021-06666-7.

36. Nagalingam A.P., Yuvaraj H.K., Yeo S.H. Synergistic effects in hydrodynamic cavitation abrasive finishing for internal surface-finish enhancement of additive-manufactured components. *Additive Manufacturing*, 2020, vol. 33, p. 101110. DOI: 10.1016/j.addma.2020.101110.

37. Nagalingam A.P., Yeo S.H. Controlled hydrodynamic cavitation erosion with abrasive particles for internal surface modification of additive manufactured components. *Wear*, 2018, vol. 414–415, pp. 89–100. DOI: 10.1016/j.wear.2018.08.006.

38. Ma C., Andani M.T., Qin H., Moghaddam N.S., Ibrahim H., Jahadakbar A., Amerinatanzi A., Ren Z., Zhang H., Doll G.L., Dong Y., Elahinia M., Ye C. Improving surface finish and wear resistance of additive manufactured nickel-titanium by ultrasonic nano-crystal surface modification. *Journal of Materials Processing Technology*, 2017, vol. 249, pp. 433–440. DOI: 10.1016/j.jmatprotec.2017.06.038.

39. Lesyk D.A., Martinez S., Mordyuk B.N., Pedash O.O., Dzhemelinskyi V.V., Lamikiz A. Ultrasonic surface post-processing of hot isostatic pressed and heat treated superalloy parts manufactured by laser powder bed fusion. *Additive Manufacturing Letters*, 2022, vol. 3, p. 100063. DOI: 10.1016/j.addlet.2022.100063.

40. Ye Y., Zhang C., Gao L., Peng L., Liu G., Zhang Y., Tang C., Huang T., Ye C. Effect of electropulsing-assisted ultrasonic nanocrystal surface modification on microstructures and hardness of additive manufactured Inconel 718. *Engineering Failure Analysis*, 2023, vol. 153, p. 107611. DOI: 10.1016/j.engfailanal.2023.107611.

41. Xu Q., Qiu Z., Jiang D., Cai G., Yang X., Liu J., Li G. Surface properties of additively manufactured 316L steel subjected to ultrasonic rolling. *Journal of Materials Engineering and Prformance*, 2024, vol. 34 (2), pp. 1733–1742. DOI: 10.1007/s11665-024-09173-4.

42. Amanov A., Karimbaev R.M. Effect of ultrasonic nanocrystal surface modification temperature: microstructural evolution, mechanical properties and tribological behavior of silicon carbide manufactured by additive manufacturing. *Surface and Coatings Technology*, 2021, vol. 425, p. 127688. DOI: 10.1016/j.surfcoat.2021.127688.

43. Walker P., Malz S., Trudel E., Nosir S., ElSayed M.S.A., Kok L. Effects of ultrasonic impact treatment on the stress-controlled fatigue performance of additively manufactured DMLS Ti-6Al-4V alloy. *Applied Sciences*, 2019, vol. 9 (22), p. 4787. DOI: 10.3390/app9224787.

44. Maleki E., Bagherifard S., Unal O., Jam A., Shao S., Guagliano M., Shamsaei N. Superior effects of hybrid laser shock peening and ultrasonic nanocrystalline surface modification on fatigue behavior of additive manufactured AlSi10Mg. *Surface and Coatings Technology*, 2023, vol. 463, p. 129512. DOI: 10.1016/j.surfcoat.2023.129512.

45. Zhao W., Liu D., Chiang R., Qin H., Zhang X.H., Zhang H., Liu J., Ren Z., Zhang R., Doll G.L., Vasudevan V.K., Dong Y., Ye C. Effects of ultrasonic nanocrystal surface modification on the surface integrity, microstructure, and

wear resistance of 300M martensitic ultra-high strength steel. *Journal of Materials Processing Technology*, 2020, vol. 285, p. 116767. DOI: 10.1016/j.jmatprotec.2020.116767.

46. Teramachi A., Yan J. Improving the surface integrity of additive-manufactured metal parts by ultrasonic vibration-assisted burnishing. *Journal of Micro and Nano-Manufacturing*, 2019, vol. 7 (2), p. 024501. DOI: 10.1115/1.4043344.

47. Panin A.V., Kazachenok M.S., Dmitriev A.I., Nikonov A.Y., Perevalova O.B., Kazantseva L.A., Sinyakova E.A., Martynov S.A. The effect of ultrasonic impact treatment on deformation and fracture of electron beam additive manufactured Ti-6Al-4V under uniaxial tension. *Materials Science and Engineering: A*, 2022, vol. 832, p. 142458. DOI: 10.1016/j.msea.2021.142458.

48. Rozenberg L.D. *Fizika i tekhnika moshchnogo ul'trazvuka*. T. 3. *Fizicheskie osnovy ul'trazvukovoi tekhnologii* [Physics and technology of high-power ultrasound. Vol. 3. Physical foundations of ultrasonic technology]. Moscow, Nauka Publ., 1970. 689 p.

49. Sundukov S.K. Osobennosti nalozheniya ul'trazvukovykh kolebanii v protsesse svarki [Features of the superposition of ultrasonic vibrations in the welding process]. *Obrabotka metallov (tekhnologiya, oborudovanie, instrumenty) = Metal Working and Material Science*, 2022, vol. 24, no. 2, pp. 50–66. DOI: 10.17212/1994-6309-2022-24.2-50-66.

50. Prikhod'ko V.M. *Ul'trazvukovye tekhnologii pri proizvodstve i remonte avtotraktornoi tekhniki* [Ultrasonic technologies in the production and repair of automotive equipment]. Moscow, Tekhpoligraftsentr Publ., 2000. 252 p. ISBN 5-900095-16-9.

51. Fatyukhin D.S., Nigmetzyanov R.I., Prikhodko V.M., Sukhov A.V., Sundukov S.K. A comparison of the effects of ultrasonic cavitation on the surfaces of 45 and 40kh steels. *Metals*, 2022, vol. 12 (1), p. 138. DOI: 10.3390/met12010138.

Conflicts of Interest

The authors declare no conflict of interest.

© 2025 The Authors. Published by Novosibirsk State Technical University. This is an open access article under the CC BY license (http://creativecommons.org/licenses/by/4.0).